Generation of optical signal and terahertz idler photons by spontaneous parametric down-conversion

G. Kh. Kitaeva,[1] V. V. Kornienko,[1,2] A. A. Leontyev,[1] and A. V. Shepelev[3]
[1]*Faculty of Physics, Lomonosov Moscow State University, Moscow 119991, Russia*
[2]*Dukhov All-Russia Research Institute of Automatics (VNIIA), Department 0179, Moscow 127055, Russia*
[3]*Department of Physics, Gubkin Russian State University of Oil and Gas, Moscow 119991, Russia*

(Received 4 July 2018; published 27 December 2018)

Frequency-angular characteristics of signal and idler photons generated under spontaneous parametric down-conversion are studied in a strongly frequency nondegenerate regime, without paraxial approximation, accounting for possible inherent absorption of idler waves in a nonlinear crystal, classical thermal field fluctuations, and the multimode character of parametric interaction induced by transverse spatial limitation of the pump beam. Spatial limitation is shown to lead to a huge increase in angular divergence of the idler photons generated at terahertz frequencies. General expressions are obtained for the frequency-angular sensitivity function of the nonlinear-optical terahertz wave detector and for power densities of the signal and idler photon fluxes. The absorption-induced difference in the parametric conversion coefficients for the noise and externally incident radiation of the idler frequency is shown to be described by approximately the same loss factor for all active spatial idler modes. Two different parametric contributions of the internal thermal noise to the number of output idler photons were revealed with different dependence on the idler-wave absorption. Expressions for the loss factors, which describe absorption-induced effects in signal and idler channels, are obtained and shown to be turning into one another by changing the sign of the absorption coefficient. Relative contribution of thermal and quantum field fluctuations into the intrinsic radiation of a nonlinear crystal at signal and idler frequencies is analyzed accounting for the crystal absorption properties.

DOI: 10.1103/PhysRevA.98.063844

I. INTRODUCTION

Parametric down-conversion (PDC) is a well-known and comprehensively studied quantum optical effect, which is widely used for generation of entangled photons and squeezed vacuum states in actual optical quantum information schemes [1]. As it was first shown in 1967 [2–5], PDC can be easily arranged by laser pumping of any medium with quadratic nonlinear-optical response. By this way, the quantum-correlated pairs of so-called signal (at frequencies ω_s higher than half of the pump frequency ω_p, $\omega_s \geqslant \omega_p/2$) and idler (at frequencies $\omega_i = \omega_p - \omega_s$ below this level, $\omega_i \leqslant \omega_p/2$) photons are generated in a wide spectral range. Nevertheless, although the correlated photons in pairs may address completely different spectral ranges, only the optical part of their spectrum attracts the main part of the attention [6]. Usually the PDC processes, both in the low-gain (spontaneous PDC [7]) and high-gain (generation of twin beams [8]) limits, are considered in the frequency-degenerate case when $\omega_s = \omega_i = \omega_p/2$, or in the slightly nondegenerate case ($\omega_s > \omega_i$) when the difference between signal and idler frequencies is less than the spectral band of optical transmission of the nonlinear crystal. This seems reasonable, since some additional increase of $\omega_s - \omega_i$ shifts ω_i out from the optical transmission diapason to a range of crystal phonon absorption, where quantum purity of the biphoton pairs is violated. However, by further decreasing ω_i one passes the range of high phonon absorption and comes to the lowest phonon-polariton branch of the crystal dispersion law $\omega_i(k_i)$. In the lowest-frequency part of this branch, practically at $\omega_i \leqslant 3$ THz, the influence of phonon resonances is minimal and absorption coefficients become reasonably small. The PDC-generated pairs consist of two photons again, but the frequency of a signal photon is just close to the pump frequency, while the idler photon frequency hits the terahertz range [9–12]. This regime can be referred to as strongly nondegenerate PDC.

The terahertz frequency (THz) range has been attracting considerable interest due to promising applications in various areas including spectroscopy, imaging, nondestructive evaluation, and communication [13]. Ways of exploiting high-capacity THz channels are becoming a problem of growing importance for wireless THz communications [14]. Studies of resonance interaction of THz radiation with matter started at a novel experimental level [15]. Nevertheless, promotion of any analogs of quantum-optical technologies into this range is still slow. The strongly nondegenerate PDC may be useful for constructing a "quantum bridge" between microwave and optical ranges. The study of its specific properties and possible applications has almost just begun. Primary calculations of the second-order correlation functions were performed accounting for possible inherent absorption and concomitant noise at THz frequencies but without taking into account the multimode character of the strongly nondegenerate PDC [11,12]. A number of our previous works were devoted to the possibility of application of strongly nondegenerate PDC for quantum calibration of the spectral brightness of the THz sources [16,17]. But again, a proper attention was

not paid to the possibility of parametric coupling between one signal mode and a number of plane idler modes. The multimode effects appear due to transverse spatial finiteness of the nonlinear volume—that part of a nonlinear crystal where the parametric process proceeds [18]. They can be insignificant for both optical signal and idler modes, but are quite important, namely, in the strongly nondegenerate regime, when the nonlinear volume cross-section is not much larger than the idler wavelength. This was shown recently by studying the optical-terahertz biphoton wave function [19]. However, calculations were performed within the limited scope of this method, and inherent absorption of the nonlinear crystal at THz frequencies was neglected.

In this paper we extend the task and theoretically analyze numbers of photons and spectral power densities both at signal and idler frequencies in a more general case. The strongly nondegenerate spontaneous PDC is considered, taking into account (a) transverse (due to the Gaussian pump beam) and longitudinal (due to the crystal length) effective spatial limitation of the nonlinear volume, (b) possible crystal absorption, and (c) presence of the thermal fields and field fluctuations at idler frequencies. All this is done using the "polariton" generalized Kirchhoff law [20]. This method was proposed by Klyshko for PDC in a nonlinear crystal with inherent absorption at idler frequencies.

The rest of the paper is organized as follows. We begin with a general description of this rather rarely used theoretical approach in Sec. II. Then, in Sec. III, expressions for the scattering matrix elements of a lossy nonlinear medium are obtained in nonparaxial and low-gain approximations accounting for the multimode effect. These expressions are substituted further into the generalized Kirchhoff law for the numbers of signal and idler photons per mode. Two types of readings of a narrow-band signal photodetector, the spontaneous and induced ones, are analyzed in Sec. IV. Characteristics of idler radiation under thermal equilibrium conditions, i.e., when the temperatures of the crystal and of the incoming radiation coincide, are studied in Sec. V. Contributions of thermal and quantum field fluctuations to the numbers of generated signal and idler photons are analyzed and compared in Sec. VI. Final conclusions and summary are given in the last section.

II. NONLINEAR GENERALIZED KIRCHHOFF LAW

Usually, characteristics of the low-gain ("spontaneous") PDC process are calculated using the biphoton wave function [1,7]. However, it is easy to do when the losses in the nonlinear medium are negligible. If the intrinsic absorption effects are essential, the biphoton field is in a mixed state and one has to take into account its interaction with an environment. This interaction can be accounted for in the second approach, which is based on solving the Heisenberg equations for evolution of the field operators [21]. Apart from the dissipation terms, the special Langevin noise operators are designed and introduced into these equations [11,21–24]. After solving these Heisenberg equations, the second-order field moments (the numbers of photons in idler and signal modes, as well as the idler-signal field correlation moments) are calculated by averaging over the initial nonperturbed state of the mixed system. In some cases the same results can be obtained using the logic of the fluctuation-dissipation theorem [25] without direct modeling of the Langevin terms. In the 1980s Klyshko formulated the so-called generalized nonlinear Kirchhoff law [20] which makes it possible to determine the second-order field moments in the case when one knows the evolution of the *mean values* of the field operators. In contrast to equations for operators, these equations are similar to classical equations for slowly varying field amplitudes and, due to averaging, do not include the Lagevin terms. This generalized nonlinear Kirchhoff law (GKL) is applicable to PDC in the medium with inherent losses at idler frequencies while being transparent at signal frequencies. Klyshko obtained it after studying the kinetic equation for evolution of the characteristic operator $\hat{\chi}(v_s, v_i) = e^{v_s a_s^+ + v_i a_i^+} e^{-v_s^* a_s - v_i^* a_i}$. By averaging, taking derivatives, and solving the obtained equations for the first- and second-order field moments he obtained relations between the moments at the input and output of the nonlinear medium. Finally, the GKL was presented by a set of equations (p. 356 in [20]) for second-order moments expressed in terms of elements of the scattering matrix of a nonlinear medium.

Our paper relies on the two of the GKL equations. The first one depicts the mean number of photons in a signal mode $\langle N_s(L)\rangle$ taken at the output of a nonlinear crystal:

$$\langle N_s(L)\rangle = \sum_{s'} |U_{ss'}|^2 \langle N_{s'}(0)\rangle + \sum_{i'} |U_{si'}|^2 (\langle N_{i'}(0)\rangle - \langle N_T\rangle) + \left(\sum_{s'} |U_{ss'}|^2 - 1\right)(1 + \langle N_T\rangle). \quad (1)$$

The second GKL equation depicts the same number in an idler mode $\langle N_i(L)\rangle$:

$$\langle N_i(L)\rangle = \sum_{i'} |U_{ii'}|^2 (\langle N_{i'}(0)\rangle - \langle N_T\rangle) + \sum_{s'} |U_{is'}|^2 \langle N_{s'}(0)\rangle + \langle N_T\rangle + \sum_{s'} |U_{is'}|^2 (1 + \langle N_T\rangle). \quad (2)$$

Since Klyshko considered absorption effects for idler waves only, the input-output relations have different forms for signal and idler photons. Here, $\langle N_{s'}(0)\rangle$ and $\langle N_{i'}(0)\rangle$ are the numbers of photons in the modes of signal and idler frequencies at the input of the crystal. These mode populations can be treated as values of spectral brightness of external sources given in quantum units—"numbers of photons per mode" [20]. Thermal field fluctuations at idler-wave frequencies are presented by Planck's factor:

$$\langle N_T\rangle = \frac{1}{\exp(\hbar\omega_i/k_B T) - 1}, \quad (3)$$

where T is the crystal temperature. $U_{ab'}$ $(a, b = s \text{ or } i)$ are scattering matrix elements.

The first and second terms in both GKL Eqs. (1) and (2) describe classical effects of parametric amplification (via $|U_{ss'}|^2\langle N_{s'}(0)\rangle$ or $|U_{ii'}|^2\langle N_{i'}(0)\rangle$) and frequency conversion (via $|U_{si'}|^2\langle N_{i'}(0)\rangle$ or $|U_{is'}|^2\langle N_{s'}(0)\rangle$) induced in the presence of external radiation. It is noteworthy that, in the case of idler radiation, only a difference $\langle N_{i'}(0)\rangle - \langle N_T\rangle$ between the external source brightness and effective brightness of thermal fluctuations $\langle N_T\rangle$ is amplified or converted. Indeed,

if the idler source brightness is the same as the brightness of crystal thermal emission, the external radiation is equivalent to thermal equilibrium radiation of the surrounding objects. Subtraction of the crystal equilibrium thermal radiation $\langle N_T\rangle$ in the two first terms of GKL Eqs. (1) and (2) can be treated as a result of mutual interplay of incoming (from the surrounding objects) and outgoing (from the crystal) radiation fluxes at the entrance of the nonlinear crystal.

The residual GKL terms are responsible for spontaneously emitted photons. Equation (1) contains only one term of such type, but Eq. (2) includes also the crystal thermal emission $\langle N_T\rangle$ which appears at the crystal exit in full compliance with the linear Kirchhoff law. Even at room temperatures, the classical thermal fluctuations can play a significant role at low idler-wave frequencies in the strongly nondegenerate regime.

The scattering matrix $\hat{U}$ connects linearly first-order correlation functions, i.e., averages of idler and signal field operators, at the input ($z=0$) and at the output ($z=L$) of the nonlinear crystal:

$$\langle a_s^\dagger(L)\rangle = \sum_{s'} U_{ss'}\langle a_{s'}^\dagger(0)\rangle + \sum_{i'} U_{si'}\langle a_{i'}(0)\rangle,$$
$$\langle a_i^\dagger(L)\rangle = \sum_{s'} U_{is'}\langle a_{s'}(0)\rangle + \sum_{i'} U_{ii'}\langle a_{i'}^\dagger(0)\rangle. \quad (4)$$

In what follows, the primed and unprimed indices denote different plane-wave modes of signal (s) and idler (i) radiation. In the case of a nonabsorptive nonlinear crystal, elements $U_{ab'}$ coincide with the coefficients which describe the Bogolyubov transformations [8] and connect operators instead of their average values. They are usually found by solving Heisenberg equations for spatially varying field operators. In the simplest case of lossless and spatially transverse-unlimited nonlinear interaction volume (the plane-wave pump, a transversely infinite crystal, and no reflections at the crystal boundaries) the Heisenberg equations take the forms [8,26,27]

$$\frac{da_s(z)}{dz} = i\gamma_{si}a_i^+(z)e^{i\Delta k_z\cdot z},$$
$$\frac{da_i^+(z)}{dz} = -i\gamma_{si}{}^*a_s(z)e^{-i\Delta k_z\cdot z}. \quad (5)$$

Here and below, the z axis is directed normally to a layer-shaped crystal; $\Delta k_z \equiv (\mathbf{k}_s+\mathbf{k}_i-\mathbf{k}_p)_z$ is a longitudinal mismatch between the wave vectors of the pump ($\mathbf{k}_p$), signal ($\mathbf{k}_s$), and idler ($\mathbf{k}_i$) plane waves;

$$\gamma_{si} \equiv \frac{2\pi\omega_s\omega_i}{c^2\sqrt{k_{sz}k_{iz}}}E_p\chi^{(2)}$$

is a specific gain per unit length; $\chi^{(2)}$ is an effective value of the crystal second-order susceptibility; E_p is a classical pump field amplitude. We consider a monochromatic pump at frequency ω_p, so that for each pair of signal and idler frequencies ω_s and ω_i the strict relation $\omega_p=\omega_s+\omega_i$ is satisfied.

Considering the absorptive nonlinear medium one has to include into the Heisenberg Eqs. (5) additional terms describing not only the attenuation of the fields during their propagation along the crystal but also the noise field operators that are responsible for the absorbing reservoir [11,21–24]. However, to find the scattering matrix elements we do not have to solve the equations for evolution of operators. Due to averaging, the impact of the noise field into such relations vanishes, and finally the equations take the forms

$$\frac{d\langle a_s(z)\rangle}{dz} = i\gamma_{si}\langle a_i^+(z)\rangle e^{i\Delta k_z\cdot z} - \mu_s\langle a_s(z)\rangle,$$
$$\frac{d\langle a_i^+(z)\rangle}{dz} = -i\gamma_{si}{}^*\langle a_s(z)\rangle e^{-i\Delta k_z\cdot z} - \mu_i\langle a_i^+(z)\rangle, \quad (6)$$

that are similar to classical wave equations for slowly varying field amplitudes in an absorptive crystal. Attenuation of the idler ($a=i$) and signal ($a=s$) waves is taken into account through the factors $\mu_a \equiv \frac{\alpha_a}{2\cos\vartheta_a}$. μ_a are proportional to the crystal intensity absorption coefficients α_a and take into consideration the different paths of propagation for waves generated at different angles to the crystal normal Z. Equations (6) are valid for the spatially transverse-unlimited nonlinear volume. In this case, the exact transverse phase-matching condition must be fulfilled for the transverse components of the pump, idler, and signal wave vectors. This guarantees one by one interaction between signal and idler modes, i.e., only one idler plane mode is parametrically connected with one plane signal mode, and each submatrix $U_{ab'}$ consists of only one element. Equations (6) admit analytical solution [28] and explicit expressions for the scattering matrix elements can be written as

$$U_{ss} = e^{-\rho_{si}}\left(\cosh\beta_{si} + \rho_{si}\frac{\sinh\beta_{si}}{\beta_{si}}\right),$$
$$U_{si} = iL\gamma_{si}e^{-\rho_{si}}\frac{\sinh\beta_{si}}{\beta_{psi}},$$
$$U_{ii} = e^{-\rho_{si}*}\left(\cosh\beta_{si} - \rho_{si}\frac{\sinh\beta_{si}}{\beta_{si}}\right),$$
$$U_{is} = -iL\gamma_{si}{}^*e^{-\rho_{si}*}\frac{\sinh\beta_{si}}{\beta_{si}}, \quad (7)$$

with

$$\beta_{si} \equiv \sqrt{(L\gamma_{si})^2+\eta_{si}{}^2},\ \eta_{si} \equiv (\mu_i-\mu_s-i\Delta k_z)L/2,$$
$$\rho_{si} \equiv (\mu_i+\mu_s-i\Delta k_z)L/2.$$

Experimentally, the transverse dimensions of the nonlinear volume are limited by the cross-section of the pump beam. The model of transverse-unlimited volume can be invalid in the case of the strongly nondegenerate PDC, since the pump beam waist is not much larger than the idler wavelength in this regime. In order to consider the multimode nature of the parametric interaction, in the next section we first calculate the scattering matrix for a PDC with a spatially limited pump beam.

III. SCATTERING MATRIX OF AN ABSORPTIVE CRYSTAL IN THE CASE OF A TRANSVERSE-LIMITED PUMP BEAM

The pump field distribution will be taken into account in a Gaussian form:

$$E_p(\mathbf{r}_\perp, z, t) = A_0 e^{-\mathbf{r}_\perp{}^2/w_p^2}e^{ik_{pz}z-i\omega_p t}.$$

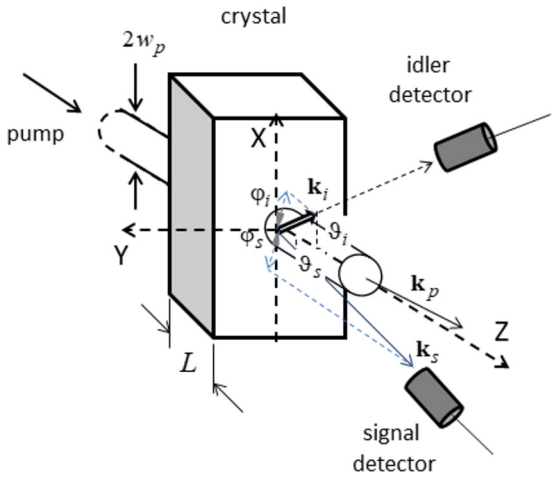

FIG. 1. Schematics of mutual orientation of signal, idler, and pump plane waves in a nonlinear crystal.

The crystal is considered to be no longer than the focal depth, so that its spatial decomposition by plane waves (modes) takes a simple form:

$$E_p(\mathbf{r}_\perp, z, t) = \int \frac{A_0 w_p^2}{4\pi} e^{-\frac{w_p^2 \mathbf{k}_{p\perp}^2}{4}} e^{i\mathbf{k}_{p\perp}\mathbf{r}_\perp + ik_{pz}z - i\omega_p t} d\mathbf{k}_{p\perp}. \tag{8}$$

Here, w_p is a pump beam waist, $\mathbf{r}_\perp$ and z characterize spatial coordinates along directions transverse and parallel to the normal to the crystal input surface correspondingly (Fig. 1), and $\mathbf{k}_{p\perp}$ and k_{pz} are transverse and longitudinal projections for different pump plane-wave components that propagate at different polar angles ϑ_p to the crystal normal so that $|\mathbf{k}_{p\perp}| = k_p \sin\vartheta_p$ and $k_{pz} = k_p \cos\vartheta_p$. $k_p = \omega_p n_p/c$, where n_p is the crystal refractive index at the pump frequency ω_p. Due to the multimode pump beam structure the one-to-one correspondence of signal and idler modes is violated and equations for evolution of averaged operators become more complicated:

$$\frac{d\langle a_s(z)\rangle}{dz} + \mu_s \langle a_s(z)\rangle = i \sum_{i'} \int \gamma_{si'} \langle a_{i'}^+(z)\rangle e^{i\Delta k_{z,psi'}z} \delta(\mathbf{k}_{s\perp} + \mathbf{k}'_{i\perp} - \mathbf{k}_{p\perp}) d\mathbf{k}_{p\perp}, \tag{9a}$$

$$\frac{d\langle a_i^+(z)\rangle}{dz} + \mu_i \langle a_i^+(z)\rangle = -i \sum_{s'} \int \gamma_{s'i}{}^* \langle a_{s'}(z)\rangle e^{-i\Delta k_{z,ps'i}z} \delta(\mathbf{k}_{s'\perp} + \mathbf{k}_{i\perp} - \mathbf{k}_{p\perp}) d\mathbf{k}_{p\perp}. \tag{9b}$$

Now any signal mode [characterized by some index s in Eq. (9a)] can interact nonlinearly with a spectrum of idler modes (indexed by i') via various plane pump modes (indexed by p) if the corresponding transverse phase mismatch $\Delta k_{\perp psi'} \equiv (\mathbf{k}_s + \mathbf{k}'_i - \mathbf{k}_p)_\perp$ is zero. The same is valid for any idler mode [labeled by i in Eq. (9b)] that is parametrically coupled to a spectrum of signal modes. The coupling efficiency depends on the pump mode amplitudes

$$E_p(\mathbf{k}_{p\perp}) = \frac{A_0 \pi w_p^2}{S} e^{-\frac{w_p^2 \mathbf{k}_{p\perp}^2}{4}},$$

which are included now in the gain coefficients γ_{si}. Here, S is a cross-sectional area of the crystal. Due to exact transverse phase matching between the plane-wave components, integration over pump modes means integration over pairs of idler and pump modes in Eq. (9a), and pairs of signal and pump modes in Eq. (9b).

The system of Eqs. (9a) and (9b) can be solved analytically in the low-gain approximation, when $L\gamma_{si} \ll 1$ and PDC has the character of spontaneous parametric down-conversion (SPDC). Results for the average field operators at the crystal output, presented in the form of Eq. (4), give explicit expressions for the scattering matrix elements:

$$U_{ss'} = e^{-\mu_s L}\delta_{ss'} + \sum_i \frac{L^2 \gamma_{si}\gamma_{s'i}{}^*}{2\eta_{si}} e^{-\rho_{si}} \times \left[e^{\eta_{s'i}} \frac{\sinh(\eta_{s'i} - \eta_{si})}{\eta_{s'i} - \eta_{si}} - \frac{\sinh\eta_{si}}{\eta_{si}} \right], \tag{10a}$$

$$U_{si'} = iL\gamma_{i's} e^{-\rho_{i's}} \frac{\sinh\eta_{i's}}{\eta_{i's}}, \tag{10b}$$

$$U_{is'} = -iL\gamma_{s'i}{}^* e^{-\rho^*_{s'i}} \frac{\sinh\eta_{s'i}}{\eta_{s'i}}, \tag{10c}$$

$$U_{ii'} = e^{-\mu_i L}\delta_{ii'} - \sum_s \frac{L^2 \gamma_{si}{}^* \gamma_{si'}}{2\eta_{si'}} e^{-\rho^*_{si}} \times \left[e^{-\eta_{si'}} \frac{\sinh(\eta_{si'} - \eta_{si})}{\eta_{si'} - \eta_{si}} - \frac{\sinh\eta_{si}}{\eta_{si}} \right]. \tag{10d}$$

Here, the factors η_{si}, γ_{si}, and ρ_{si} depend only on parameters of signal and idler modes, whereas the parameters of the corresponding plane pump mode are determined by transverse phase-matching conditions. Because of the nonparaxial character of strongly nondegenerate PDC, we have to take into account angles of the wave vectors that stand in expressions for corresponding gain coefficients γ_{si}. These coefficients can vary drastically for various triplets of plane signal, idler, and pump plane modes taken even at the same signal, idler, and pump frequencies.

Following Klyshko's procedure, in the next sections the scattering matrix elements from Eqs.(10) will be substituted into the GKL Eqs. (1) and (2). Since GKL is formulated only for nonlinear media transparent at signal frequencies, further, we take $\mu_s = 0$.

IV. SIGNAL PHOTONS AND NONLINEAR-OPTICAL DETECTION OF AN EXTERNAL IDLER RADIATION

To figure out the number of photons in any output signal mode we use the GKL Eq. (1). Parametric amplification of an external signal is not included in our task and it is further assumed that $\langle N_{s'}(0)\rangle = 0$. The second term in Eq. (1) describes the classical effect of difference frequency generation (DFG) at signal frequency $\omega_s = \omega_p - \omega_i$ that occurs when two waves of frequencies ω_p and ω_i are incident on a nonlinear crystal. By substituting Eq. (10b) for the nondiagonal scattering

matrix elements $U_{si'}$ into this GKL term, we obtain expression for $\langle N_s^{\mathrm{DFG}}(L)\rangle$ in the low-gain limit

$$\left\langle N_s^{\mathrm{DFG}}(L)\right\rangle = \sum_i g_{si}(\langle N_i(0)\rangle - \langle N_T\rangle) \tag{11}$$

with the parametric gain coefficient

$$g_{si} \equiv |U_{si}|^2 = |U_{is}|^2 = (L\gamma_{si})^2 e^{-\mu_i L}\left|\frac{\sinh\eta_{si}}{\eta_{si}}\right|^2. \tag{11a}$$

g_{si} characterizes the level of nonlinear-optical interaction in a particular pair of signal and idler waves.

The third term in GKL Eq. (1) corresponds to a pure spontaneous signal, which may be seen without any special external idler- or and signal-wave source, when the temperatures of the nonlinear medium and the surrounding objects coincide. Comparison with the DFG term shows that the spontaneous signal can be treated as a result of parametric conversion of classical thermal ($\langle N_T\rangle$) and quantum (with effective brightness 1 photon/mode) field fluctuations at idler frequencies. By substituting Eq. (10a) into the third term in Eq. (1), taking $\mu_s = 0$, and accounting for the terms up to ${\gamma_{is}}^2$, we obtain the brightness of the spontaneous signal in the form

$$\left\langle N_s^{\mathrm{Spon}}(L)\right\rangle = \sum_i g_{si}^{\mathrm{Spon}}(1 + \langle N_T\rangle) \tag{12}$$

with another gain coefficient:

$$g_{si}^{\mathrm{Spon}} \equiv (L\gamma_{si})^2\left(\frac{2\eta_{si} - 1 + e^{-2\eta_{si}}}{(2\eta_{si})^2} + \mathrm{c.c.}\right). \tag{12a}$$

Here, g_{si}^{Spon} characterizes the nonlinear-optical contribution of quantum and thermal idler field fluctuations to the number of optical signal photons. It is easy to see that the gain coefficients for fluctuations (g_{si}^{Spon}) and external radiation (g_{si}) coincide only if the absorption effects can be neglected:

$$g_{si}^{\mathrm{Spon}}\big|_{\mu_i=0} = g_{si}\big|_{\mu_i=0} = (L\gamma_{si})^2 \mathrm{Sinc}^2\frac{\Delta k_z L}{2}.$$

Accounting for strict relation $\omega_s = \omega_p - \omega_i$, summation over all spatial idler modes $\sum_i$ will be further substituted by integration over idler mode solid angles as $\sum_i \to \frac{S}{(2\pi)^2}\int {k_i}^2 d\Omega_i$. Since the crystal is considered to be linearly transparent at signal frequencies in GKL, $\eta_{si} = \rho_{si} = -i(\Delta k_z + i\mu_i)L/2$ in Eq. (11) and below. Here, $\Delta k_z + i\mu_i$ looks like a complex longitudinal mismatch that accounts for the imaginary part of the idler-wave vector in the form

$$k_{iz} = \frac{\omega_i n_i}{c}\cos\vartheta_i + i\frac{\alpha_i}{2\cos\vartheta_i}.$$

Let us further consider in this section the averaged readings of a narrow-band optical photodetector with quantum efficiency ξ_s that measures the signal power within the spectral band $\Delta\omega_s = \Delta\omega_i \ll \omega_i, \omega_s$ in the far zone after the crystal. The number of counts per second is calculated by integration of $\langle N_s(L)\rangle$ across the photodetector's solid angle of view:

$$P_s = \xi_s\frac{{\omega_s}^2}{(2\pi)^3 c^2}\Delta\omega_s\int S_s\langle N_s(L)\rangle d\Omega_s.$$

Here, S_s is an input area of the photodetector oriented normally to the signal radiation. In what follows its projection on the crystal output surface $S_s^{\mathrm{cr}} \equiv \frac{S_s}{\cos\vartheta_s}$ is taken into account. We consider the case when the detector's acceptance angle $\Delta\Omega_s = \sin\vartheta_s\Delta\vartheta_s\Delta\varphi_s$ is sufficiently less than the total divergence angle of signal radiation, and the photodetector receives signal waves at the angles $\vartheta_s \approx \vartheta_{s0}, \quad \varphi_s \approx \pi$ where the phase-matching conditions are almost completely fulfilled.

Taking into account Eqs. (11) and (12), one can obtain the photodetector's readings due to the induced (DFG) process as

$$P_s^{\mathrm{DFG}} = C_{\omega_s}\int S_\omega(\vartheta_{s0}, \vartheta_i, 0, \varphi_i)\left(\left\langle N_{k_i}(0)\right\rangle - \langle N_T\rangle\right) \times tg\vartheta_i d\vartheta_i d\varphi_i, \tag{13}$$

and the same readings under the spontaneous process as

$$P_s^{\mathrm{Spon}} = C_{\omega_s}\int S_\omega^{\mathrm{SPDC}}(\vartheta_{s0}, \vartheta_i, \pi, \varphi_i)(1 + \langle N_T\rangle)tg\vartheta_i d\vartheta_i d\varphi_i. \tag{14}$$

Here, the coefficient

$$C_{\omega_s} = \sigma_s\frac{\omega_s^3\omega_i^3 n_i}{8\pi c^6 n_s}\left(L\chi A_0 w_p^2\right)^2$$

describes the signal dependency on the pump power $P_p \sim (A_0 w_p)^2$, pump wavelength (since ${\omega_s}^3$ strongly depends on the choice of ω_p), the crystal refractive indices n_i, n_s and nonlinear susceptibility χ, the overall nonlinear volume $\sim L w_p^2$, and the photodetector's characteristics via

$$\sigma_s \equiv \xi_s\frac{S_{s-\mathrm{det}}^{\mathrm{cr}}}{S}\Delta\Omega_s\Delta\omega_s.$$

An effective value of the nonlinear susceptibility $\chi^{(2)}$ usually depends on the signal and idler angles itself, since it is equal to convolution of the crystal second-order susceptibility tensor $\hat{\chi}^{(2)}$ with the polarization vectors of the signal, idler, and pump modes. Here and below we take into account the $\chi^{(2)}$ dependence on the signal and idler angles in the form $\chi^{(2)} = \chi\cos\varphi_i\cos\varphi_s$.

As expected, the integrand functions in Eqs. (13) and (14) are not the same. The total effective brightness of thermal and quantum fluctuations $\langle N_T\rangle + 1$ stands in Eq. (14) instead of the excess brightness of the external idler-wave source $\langle N_i(0)\rangle - \langle N_T\rangle$ in Eq. (13), and the angular response functions S_ω^{Spon}, S_ω are different. The general expressions for the angular response functions for any signal and idler angles take the forms

$$S_\omega^{\mathrm{SPDC}}(\vartheta_s, \vartheta_i, \varphi_s, \varphi_i) = e^{-\frac{w_p^2(\mathbf{k}_{s\perp}+\mathbf{k}_{i\perp})^2}{2}}\left[\frac{1 + (i\Delta k_z - \mu_i)L - e^{(i\Delta k_z - \mu_i)L}}{(\Delta k_z + i\mu_i)^2 L^2} + \mathrm{c.c.}\right]\cos^2\varphi_s\cos^2\varphi_i \tag{15}$$

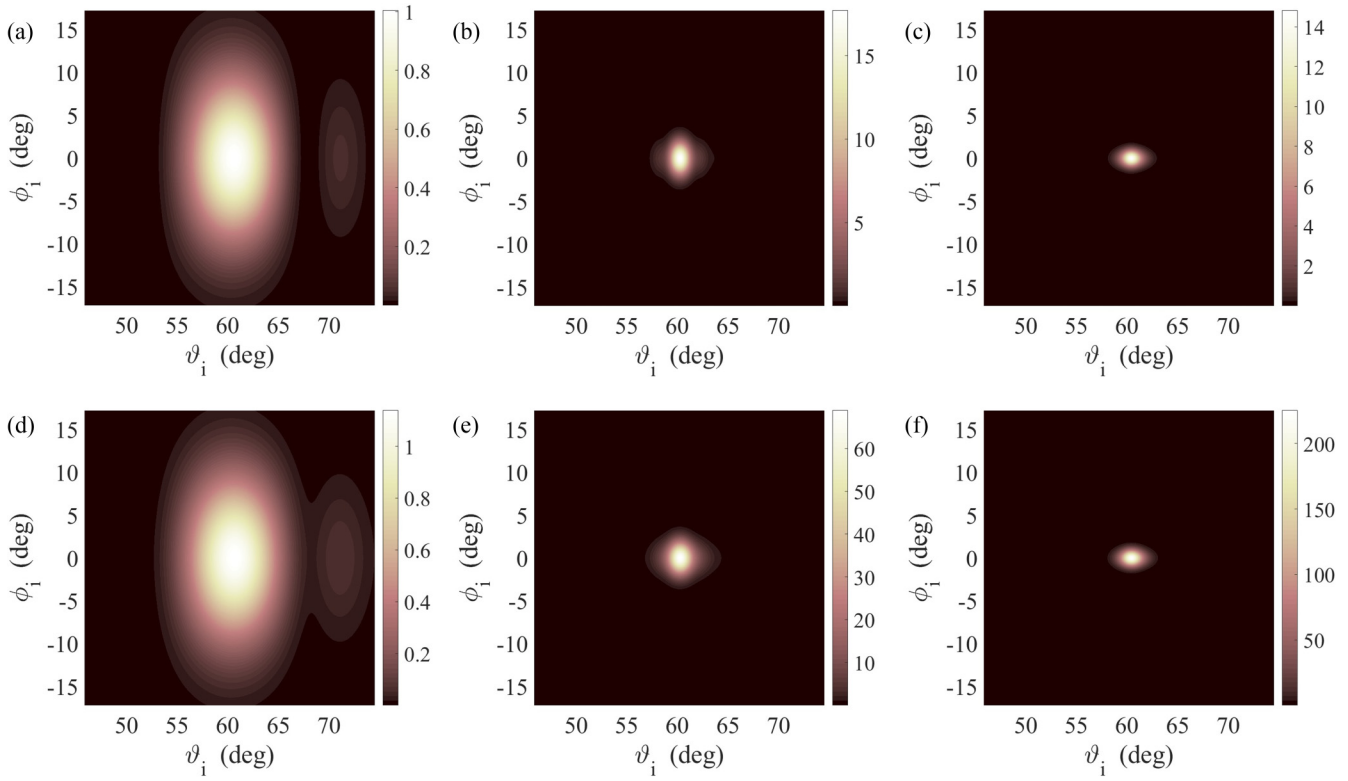

FIG. 2. Angular distributions of the sensitivity functions $S_\omega(\vartheta_{s0}, \vartheta_i, \pi, \varphi_i)\omega_i^3 tg\vartheta_i$ (a–c) and $S_\omega^{\mathrm{SPDC}}(\vartheta_{s0}, \vartheta_i, \pi, \varphi_i)\omega_i^3 tg\vartheta_i$ (d–f) calculated for type-zero parametric processes in a bulk Mg:$LiNbO_3$ crystal ($L = 5$ mm) pumped at 514.5 nm ($w_p = 1$ mm) for three idler frequencies: 0.1 THz (a, d), 0.5 THz (b, e) and 1 THz (c, f).

and

$$S_\omega(\vartheta_s, \vartheta_i, \varphi_s, \varphi_i) = e^{-\frac{w_p^2(\mathbf{k}_{s\perp}+\mathbf{k}_{i\perp})^2}{2}} e^{-\mu_i L} \left| \frac{\sinh[(i\Delta k_z - \mu_i)L/2]}{(i\Delta k_z - \mu_i)L/2} \right|^2 \cos^2\varphi_s \cos^2\varphi_i. \quad (16)$$

Figures 2(a)–2(c) and 2(d)–2(f) show examples of idler angular distributions $S_\omega(\vartheta_{s0}, \vartheta_i, \pi, \varphi_i)\omega_i^3 tg\vartheta_i$ and $S_\omega^{\mathrm{SPDC}}(\vartheta_{s0}, \vartheta_i, \pi, \varphi_i)\omega_i^3 tg\vartheta_i$, correspondingly. They are calculated for the case of type-zero nonlinear interaction in bulk Mg:$LiNbO_3$ crystal (in this case all the fields are polarized along the polar c axis of the crystal, parallel to the y axis in Fig. 1), the pump wavelength 514.5 nm, and three idler frequencies 0.1, 0.5, and 1 THz. $L = 5$ mm, and $w_p = 1$ mm. The phase-matching angle ϑ_{i0} changes between 60.28 and 60.42° in the considered case. The data on extraordinary refractive index dispersion of Mg-doped congruent lithium niobate crystal were taken from [29] for the visible range and from [30] for the terahertz range. The azimuthal angles $\varphi_{i,s}$ are counted from the x axis (Fig. 1) so that the phase-matching angle is taken as $\varphi_{i0} = 0$ and corresponds to idler-wave propagation in the plane of signal and pump wave vectors. The size of bright spots in Fig. 2 centered around the phase-matching direction ϑ_{i0}, φ_{i0} provides insight on the angular diversity of all the idler waves contributing to the parametric generation of signal photons in only one ($\vartheta_s = \vartheta_{s0}$, $\varphi_s = \pi$) direction. Due to substantial difference between signal and idler frequencies in the strongly frequency nondegenerate regime, the angular diversity of the idler waves is rather high. However, it decreases when the idler radiation frequency becomes greater, as it is illustrated by Fig. 2.

Reduction of the angular diversity can be done also by increasing the dimensions of the nonlinear volume. Figure 3 shows spectral dependences of the polar angular width

$$\Delta\vartheta_i = \frac{\int S_\omega(\vartheta_{s0}, \vartheta_i, \pi, 0) tg\vartheta_i d\vartheta_i}{S_\omega(\vartheta_{s0}, \vartheta_{i0}, \pi, 0) tg\vartheta_{i0}}$$

and of the azimuthal angular width

$$\Delta\varphi_i = \frac{\int S_\omega(\vartheta_{s0}, \vartheta_{i0}, \pi, \varphi_i) d\varphi_i}{S_\omega(\vartheta_{s0}, \vartheta_{i0}, \pi, 0)}$$

for various spatial parameters (crystal length L and pump beam radius w_p). Within the considered range of parameters, the azimuthal angle $\Delta\varphi_i$ is practically insensitive to the crystal length and depends mostly on the pump beam radius if the idler frequency is fixed. At low frequencies the opposite effect is observed for the polar angular aperture $\Delta\vartheta_i$: it depends basically on the crystal length. Nevertheless, the absorption coefficient increases with frequency and, starting from some frequency values, the crystal length loses its significance in comparison with the length of an idler-wave free path in a

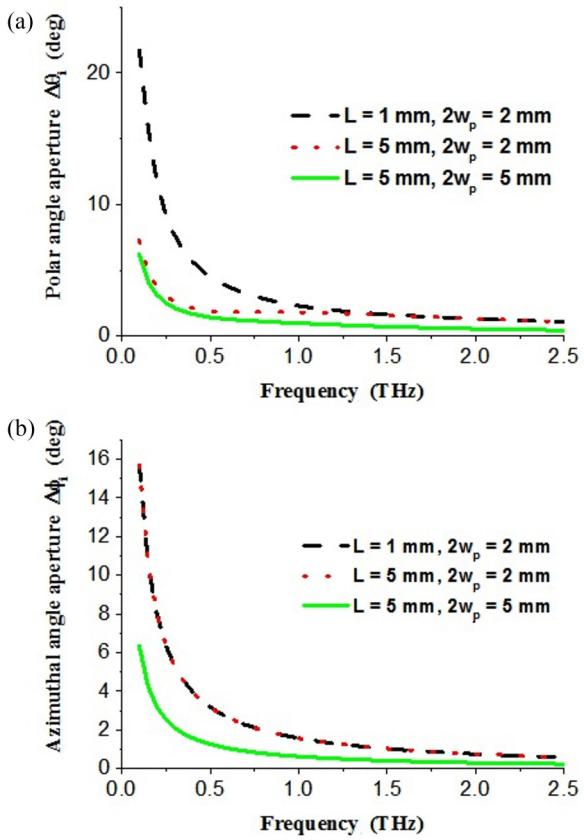

FIG. 3. Dependences of polar (a) and azimuthal (b) angle apertures of the terahertz detector based on frequency up-conversion in Mg:$LiNbO_3$ crystals of different lengths (1 mm for the dashed black lines and 5 mm for the dotted red and solid green lines) pumped by 514.5-nm Gaussian laser beams with diameters 2 mm (dashed black and dotted red lines) and 5 mm (solid green lines).

crystal. If w_p is still less than L, w_p starts to determine $\Delta\vartheta_i$ instead of L, as it is seen in Fig. 3(a) at frequencies above 1.2 THz. At frequencies higher than the range taken in Fig. 3, absorption effects become dominant.

Comparison between the functions which describe sensitivities to external idler radiation [S_ω, Figs. 2(a)–2(c)] and to internal fluctuations of the idler field [S_ω^{Spon}, Figs. 2(d)–2(f)] shows that their angular shapes are quite similar provided the absorption coefficients have reasonably moderate values ($\mu_i \leqslant 1$). At the same time, the absolute values of these functions could differ noticeably if μ_i is not vanishingly small. This takes place due to fundamentally different impacts of absorption effects on the processes of parametric conversion of internal fluctuations and externally incident idler waves. Successfully, this difference remains quite the same for all angles of idler modes involved in the parametric processes. This fact is clearly illustrated in Fig. 4. Here, the exact frequency dependence of the loss factor κ_s is calculated using its integral definition:

$$\kappa_s \equiv \frac{\int S_\omega^{\mathrm{SPDC}}(\vartheta_s,\vartheta_i,\varphi_s,\varphi_i)tg\vartheta_i d\vartheta_i d\varphi_i}{\int S_\omega(\vartheta_s,\vartheta_i,\varphi_s,\varphi_i)tg\vartheta_i d\vartheta_i d\varphi_i} = \frac{\int g_{si}^{\mathrm{Spon}} d\vartheta_i d\varphi_i}{\int g_{si} d\vartheta_i d\varphi_i}. \tag{17}$$

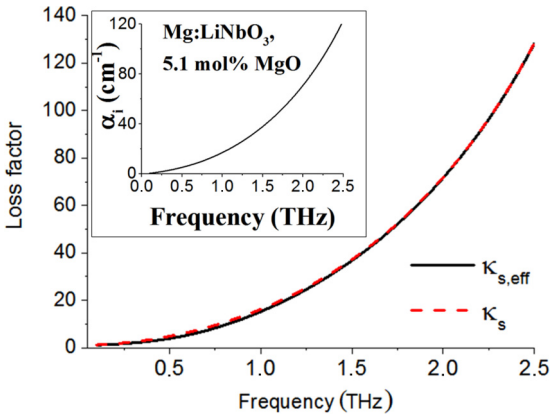

FIG. 4. Spectral behavior of the THz-loss factors which account for different contributions of external idler radiation and internal idler-field fluctuations of the same spectral brightness 1 photon/mode into the optical parametric signal in a 5 mm-long Mg:$LiNbO_3$ crystal. Dashed red line: κ_s calculated according to Eq. (17), considering that both the externally induced waves and internal idler-wave fields occupy the whole angular aperture of the frequency converter (w_p = 1 mm). Black solid line: $\kappa_{s,\mathrm{eff}}$ calculated by Eq. (18), i.e., taking into account the phase-matched modes only. Inset: Spectral dependence of the crystal absorption coefficient.

Spectral dependence of the approximate loss-factor value, determined as relation

$$\kappa_{s,\mathrm{eff}} \equiv \frac{S_\omega^{\mathrm{SPDC}}(\vartheta_{s0},\vartheta_{i0},\pi,0)}{S_\omega(\vartheta_{s0},\vartheta_{i0},\pi,0)},$$

is shown also. It is seen that $\kappa_{s,\mathrm{eff}}$ is close to κ_s within the whole actual range of THz frequencies characterized by moderate idler-wave crystal absorption. Coincidence is usually much better than 10% of the loss-factor value. Under phase-matching conditions

$$g_{si}^{\mathrm{Spon}}\big|_{\Delta k_z=0} = 2(\gamma_{si}L)^2\frac{\mu_i L - 1 + e^{-\mu_i L}}{(\mu_i L)^2}$$

and

$$g_{si}\big|_{\Delta k_z=0} = (\gamma_{si}L)^2\left(\frac{1-e^{-\mu_i L}}{\mu_i L}\right)^2,$$

so that one can easily obtain the suitable expression for precalculation of κ_s:

$$\kappa_s \approx \kappa_{s,\mathrm{eff}} = 2\frac{\mu_i L - 1 + e^{-\mu_i L}}{(1-e^{-\mu_i L})^2}. \tag{18}$$

Being determined this way, $\kappa_{s,\mathrm{eff}}$ does not depend on the direction of the signal radiation. Moreover, μ_i in Eq. (18) is taken for the phase-matched idler angle $\vartheta_i = \vartheta_{i0}$ only. Our calculations show that $\kappa_s \approx \kappa_{s,\mathrm{eff}}$ also for those signal directions where the phase-matching conditions are not satisfied exactly, i.e., where Eq. (17) is considered for $\vartheta_s \neq \vartheta_{s0}$ and $\varphi_s \neq \pi$. Figure 4 also demonstrates how fast the loss coefficient κ_s of 5-mm-long Mg:$LiNbO_3$ crystal grows when the crystal absorption coefficient increases with the terahertz idler frequency.

The fortunate coincidence of angular forms of spontaneous and induced signals allows considering separately the effects

caused by absorption, and the multimode effects caused by finiteness of the nonlinear volume. The dimension effects under strongly frequency nondegenerate parametric process lead to high angle diversity of the active idler (lower frequency) modes, whereas the loss effects manifest uniformly in all these modes. This gives a possibility to describe the numbers of spontaneous and induced signal photons by the same mode distribution of the gain coefficient g_{si} [Eq. (11a)] and account for specificity of the spontaneous signal by the loss factor $\kappa_s \approx \kappa_{s,\mathrm{eff}}$ identically for all the idler modes:

$$\left\langle N_s^{\mathrm{Spon}}(L)\right\rangle = \kappa_s \sum_i g_{si}(1+\langle N_T\rangle), \tag{19a}$$

$$\left\langle N_s^{\mathrm{DFG}}(L)\right\rangle = \sum_i g_{si}(\langle N_i(0)\rangle - \langle N_T\rangle). \tag{19b}$$

The DFG process can be used for nonlinear-optical detection of an external idler radiation via up-conversion into the optical range, where the signal radiation is easily measured by a conventional photodetector. Such method was realized recently in a number of papers for noncoherent terahertz wave detection with continuous-wave or nanosecond-pulsed lasers [31–33]. As it seen from Eq. (13), the idler angle dependence of S_ω determines the spatial resolution of such a detector [19]. Figure 3 shows examples of how the azimuthal and polar resolution scales with the dimensions of the nonlinear volume.

For a single-mode parametric frequency converter, it was shown also that the pure spontaneous signal can be used for calibration of the absolute sensitivity of such a nonlinear-optical detector [16,17,19,34]. Taking the two readings of a signal photodetector, that are the pure spontaneous signal P_s^{Spon}, obtained in the absence of any external idler-wave source, and $P_s = P_s^{\mathrm{Spon}} + P_s^{\mathrm{DFG}}$, obtained when the external source is switched on, one determines the absolute value of the external source brightness as

$$\overline{\langle N_i(0)\rangle} = \kappa_s\left(P_s/P_s^{\mathrm{Spon}} - 1\right)(1+\langle N_T\rangle) + \langle N_T\rangle. \tag{20}$$

Here, the spectral brightness is measured in quantum units "photons per mode" [20]. If necessary, it can be easily recalculated as $B_\omega = \frac{\hbar\omega_i{}^3}{(2\pi)^3 c^2}\overline{\langle N_i(0)\rangle}$ in standard photometric units. It is noteworthy that, in a multiple mode case, $\overline{\langle N_i(0)\rangle}$ determined according to Eq. (20) is the mean number of photons in all idler modes that can make contribution into the signal P_s(i.e., for which $S_\omega \neq 0$). Averaging is made over the angles of idler modes accounting for the differential sensitivity function distribution:

$$\overline{\langle N_i(0)\rangle} \equiv \frac{\int S_\omega(\vartheta_{s0},\vartheta_i,\pi,\varphi_i)\langle N_i(0)\rangle tg\vartheta_i d\vartheta_i d\varphi_i}{\int S_\omega(\vartheta_{s0},\vartheta_i,\pi,\varphi_i) tg\vartheta_i d\vartheta_i d\varphi_i}. \tag{21}$$

$\overline{\langle N_i(0)\rangle}$ coincides with $\langle N_i(0)\rangle$ in the central modes only for sufficiently isotropic radiation, which fills uniformly all the angles where the differential sensitivity has meaningful values. This property has to be taken into account, since adequate brightness estimation can be done only for sources with a large angular divergence. Thus, decreasing of the angular width of S_ω is crucial both for better spatial resolution and for more accurate absolute brightness measuring. This can be done by proper choice of the crystal length and the pump beam radius. Nevertheless, increasing the dimensions of the nonlinear volume has a limited effect since the SPDC-based calibration can be done with an appropriate accuracy when the loss factor is close to 1. This limits the spectral range of measurements in a crystal with the absorption coefficient growing at high frequencies (Fig. 4). The relations obtained in this section, mainly Eqs. (15), (16), and (18), will help us to choose optimal parameters of the nonlinear crystal according to characteristics of the terahertz wave source under detection.

Summarizing this section, we obtained general expressions for the two types of readings of a narrow-band signal photodetector, one for the spontaneous PDC and one for DFG induced by an external idler radiation. It was found that angular divergences of the idler modes depend on the idler frequency and sizes of a nonlinear volume in a very similar way for both processes. With rather high accuracy, the relation between spontaneous and induced signals can be described by one loss factor for all active directions of idler waves. These results are important for analyzing the angular sensitivity and the input angular aperture of a nonlinear terahertz wave detector, as well as for application of the SPDC method for absolute calibration of the spectral brightness.

V. IDLER PHOTONS

Now let us turn to the long-wave photons generated at idler frequencies as it is predicted by the GKL Eq. (2). In contrast to their optical (signal) partners, the idler photons are accompanied by substantial classical thermal fluctuation fields at the same frequencies, and, secondly, can be absorbed by a crystal. In this section we consider the case when there are no special sources of external input idler and signal radiation apart from thermal equilibrium idler-wave radiation of the environment. Then the total number of output idler photons is depicted by the last two terms in Eq. (2). The term $\langle N_T\rangle$ is responsible for thermal radiation of the crystal itself. The final contribution describes idler-wave photons spontaneously generated via the crystal's nonlinearity:

$$\left\langle N_i^{\mathrm{Spon}}(L)\right\rangle = \sum_s g_{si}(1+\langle N_T\rangle). \tag{22}$$

This expression has the same structure as the third term in Eq. (1), which is responsible for the spontaneous part of signal radiation. Again, since it contains effective brightness of both types of fluctuations, $1+\langle N_T\rangle$, this idler radiation can be interpreted as a result of amplification of the fluctuation fields. Here, the part proportional to 1 photon/mode depicts the pure SPDC-generated idler-wave power density. The amplification coefficients $\sum_s g_{si}$ do not coincide with the conversion coefficients $(\sum_{s'}|U_{ss'}|^2 - 1)$ in the signal part of SPDC. However, summation in Eq. (22) is carried out with the same gain coefficients g_{si} as in the DFG part of signal radiation in Eq. (11). Asymmetry appears due to crystal transparency at signal frequencies and moderate opacity at idler frequencies. If the idler-wave absorption can be neglected, the coefficients in Eqs. (11), (12), and (22) coincide.

Following the same considerations as in the previous section, we obtain an expression for the readings of a

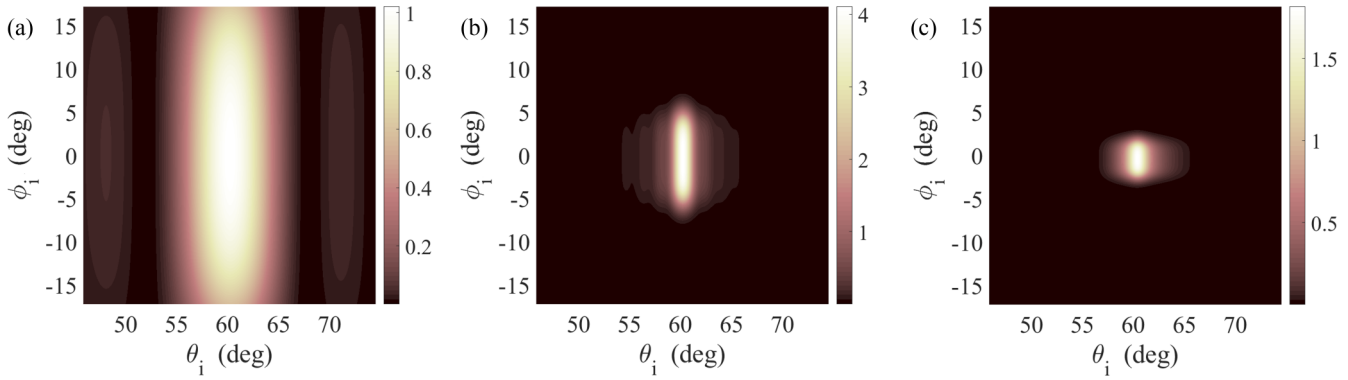

FIG. 5. Angular distributions of the idler-wave detector readings $P_i^{\mathrm{Spon}}(\vartheta_i, \varphi_i)$, calculated for the case of no external signal and no idler radiation at the input of the crystal apart from the equilibrium thermal radiation; type-zero parametric processes in a bulk Mg:$LiNbO_3$ crystal ($L = 5$ mm) pumped at 514.5 nm ($w_p = 1$ mm); and three idler frequencies: 0.1 THz (a), 0.5 THz (b), and 1 THz (c).

narrow-band idler-wave detector due to SPDC as

$$P_i^{\mathrm{Spon}}(\vartheta_i, \varphi_i) = C_{\omega_i}(1 + \langle N_T \rangle) \int S_\omega(\vartheta_s, \vartheta_i, \varphi_s, \varphi_i) \times tg\vartheta_s d\vartheta_s d\varphi_s. \tag{23}$$

Integration is made over all possible directions of the signal photons, using the same angular response function S_ω, as in the case of the DFG optical signal [see Eq. (16)]. Similarly, the angle-independent coefficient

$$C_{\omega_i} = \sigma_i \frac{\omega_s^3 \omega_i^3 n_i}{8\pi c^6 n_s} \left(L\chi^{(2)} A_0 w_p^2\right)^2$$

now accounts for parameters of the narrow-band idler-wave detector with efficiency ξ_i, input area S_i (recounted to the area parallel to the crystal output surface as $S_i^{\mathrm{cr}} \equiv \frac{S_i}{\cos\vartheta_i}$), spectral band $\Delta\omega_i$, and solid angle of reception $\Delta\Omega_i$ via

$$\sigma_i \equiv \xi_i \frac{S_i^{\mathrm{cr}}}{S} \Delta\omega_i \Delta\Omega_i.$$

As it is seen from Figs. 2 and 3, S_ω is distributed along a wide range of idler angles, and, according to Eq. (23), the SPDC-generated idler-wave photons will be spread over almost the same angles. Integration over all signal angles increases the solid angle of the idler-wave divergence. Figure 5 presents examples of angular distributions of the idler-wave detector readings $P_i^{\mathrm{Spon}}(\vartheta_i, \varphi_i)$ calculated for different idler frequencies in the same case of type-zero nonlinear interaction in bulk Mg:$LiNbO_3$ crystal pumped at 514.5 nm as in Figs. 2 and 3. It has been also taken into account that an input area of the idler-wave detector is reoriented normally to the idler-wave propagation at each change of the detection angle, so that $\sigma_i \sim 1/\cos\vartheta_i$.

In summary, in this section we analyze the number of output idler photons per mode generated under thermal equilibrium conditions, i.e., when the temperatures of the crystal and of the incoming radiation coincide:

$$\langle N_i^{\mathrm{Equil}}(L) \rangle = \langle N_i^{\mathrm{Spon}}(L) \rangle + \langle N_T \rangle. \tag{24}$$

It is found that even in the case of arbitrary idler absorption the number of SPDC generated idler photons is proportional to effective brightness of thermal and quantum fluctuations $1 + \langle N_T \rangle$ with exactly the same gain coefficient that describes the gain coefficient under DFG of signal photons. The corresponding readings of a narrow-band idler detector can be calculated using Eq. (23) by integrating the same angular sensitivity function S_ω over all possible directions of signal photons.

VI. CONTRIBUTIONS OF THERMAL AND QUANTUM FIELD FLUCTUATIONS TO SIGNAL AND IDLER PHOTONS

In the two previous sections we considered the nonlinear signals $\langle N_s^{\mathrm{Spon}}(L) \rangle$ and $\langle N_i^{\mathrm{Spon}}(L) \rangle$ generated in thermal equilibrium conditions. These conditions assume that at the input of all idler channels there is an equilibrium thermal radiation of environment with $\langle N_T \rangle$ corresponding to the crystal temperature. Let us now estimate the intrinsic radiation of the crystal singly, regardless of any nonlinear response to an external radiation whatever temperature it has.

As it follows from Eq. (1), for the *intrinsically radiated* signal photons we have

$$\langle N_s(L) \rangle = \kappa_s \left(\sum_i g_{si} \right) \langle N_q \rangle + (\kappa_s - 1) \left(\sum_i g_{si} \right) \langle N_T \rangle. \tag{25}$$

Here, $\langle N_q \rangle \equiv 1$ is introduced to mark the impact of quantum fluctuations. As it follows from the GKL Eq. (2), an analogous expression for the idler output should be built from two parts:

$$\langle N_i(L) \rangle = \langle N_i^{\mathrm{Spon}}(L) \rangle + \langle N_T \rangle \left(1 - \sum_{i'} |U_{ii'}|^2 \right). \tag{26}$$

The first part $\langle N_i^{\mathrm{Spon}}(L) \rangle$ was considered in the previous section. Concerning the second part, in the equilibrium conditions its nonlinear contribution is canceled by thermal radiation of environment, so that only $\langle N_T \rangle$ remains here in the balance. Nevertheless, it should be taken into account in its total form here, in the frames of analysis of the *intrinsically radiated* idler photons.

Using Eq. (10d) for the scattering matrix element $U_{ii'}$, we obtain that

$$\langle N_T\rangle\left(1-\sum_{i'}|U_{ii'}|^2\right)=(1-e^{-2\mu_i L})\langle N_T\rangle-e^{-2\mu_i L}\langle N_T\rangle\sum_s(L\gamma_{si})^2\left[\frac{e^{2\eta_{si}}-2\eta_{si}-1}{(2\eta_{si})^2}+\text{c.c.}\right]. \tag{27}$$

The first part on the right describes thermal radiation of the absorptive crystal, just like the linear Kirchhoff law predicts. The second term corresponds to nonlinear transformation of thermal fluctuations with a negative gain coefficient:

$$-e^{-2\mu_i L}\sum_s(L\gamma_{si})^2\left[\frac{e^{2\eta_{si}}-2\eta_{si}-1}{(2\eta_{si})^2}+\text{c.c.}\right]. \tag{27a}$$

Comparing this relation with Eq. (12a) one can see that this coefficient brings us back to the gain coefficient in the expression for spontaneously emitted signal photons, but asymmetry due to idler-wave absorption leads to some discrepancies. Once again note that in the case of zero absorption all the conversion and amplification coefficients coincide.

Following the same approach as in Sec. IV, we introduce the loss factor κ_i, which depicts the relation between the two transfer (for $\langle N_T\rangle$) coefficients at idler frequencies:

$$\kappa_i(\vartheta_i,\varphi_i)=\frac{e^{-\mu_i L}\cos^2\varphi_i\int e^{-\frac{w_p^2(\mathbf{k}_{s\perp}+\mathbf{k}_{i'\perp})^2}{2}}\left[\frac{e^{2\eta_{si}}-2\eta_{si}-1}{(2\eta_{si})^2}+\text{c.c.}\right]\cos^2\varphi_s tg\vartheta_s d\vartheta_s d\varphi_s}{\int S_\omega(\vartheta_s,\vartheta_i,\varphi_s,\varphi_i)tg\vartheta_s d\vartheta_s d\varphi_s}. \tag{28}$$

Our calculations show that, similar to $\kappa_{s,\text{eff}}$, this loss coefficient can be approximately determined taking the phase-matched directions of idler and signal waves:

$$\kappa_i(\vartheta_i,\varphi_i)\approx\kappa_{i,\text{eff}}=2\frac{e^{\mu_i L}-\mu_i L-1}{(e^{\mu_i L}-1)^2}. \tag{29}$$

Notably, this expression for $\kappa_{i,\text{eff}}$ can be converted to Eq. (18) for $\kappa_{s,\text{eff}}$ by changing a sign of the absorption coefficient, $\mu_i\to-\mu_i$, i.e.,

$$\kappa_{s,\text{eff}}(\mu_i)=\kappa_{i,\text{eff}}(-\mu_i).$$

$\kappa_{i,\text{eff}}$ rapidly goes down from one to zero when the absorption coefficient increases with frequency (see an example of the $1-\kappa_{i,\text{eff}}$ spectral dependence in Fig. 6). It should be noted that replacement of the exact κ_i by its approximate value $\kappa_{i,\text{eff}}$ can lead to a greater loss of accuracy than the same procedure in the signal range. However, this approximation substantially simplifies the analysis of relative contributions of thermal and quantum fluctuations.

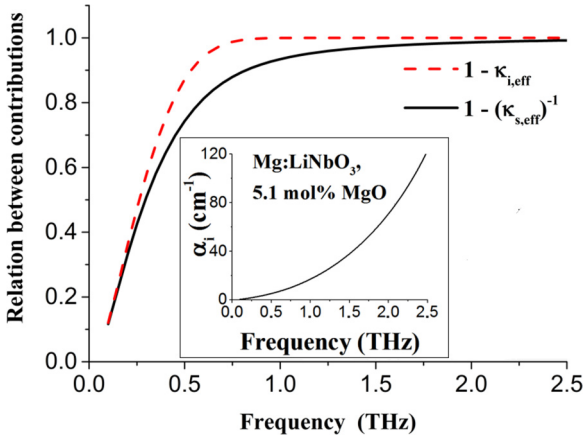

FIG. 6. Spectral behavior of the relation between contributions of thermal and quantum field fluctuations, taken at the same number of photons per mode, $\langle N_T\rangle=\langle N_q\rangle=1$, to the intrinsic pump-induced radiation at signal (black solid curve) and idler (red dashed curve) frequencies. Calculations are made for a 5-mm-long $Mg:LiNbO_3$ crystal with absorption coefficient dependence shown in the inset.

Readings of the idler-wave narrow-band detector, which correspond to this additional part of nonlinear amplification of thermal fluctuations, can be calculated as

$$P_i(\vartheta_i,\varphi_i)=C_{\omega_i}\langle N_T\rangle\kappa_i\int S_\omega(\vartheta_s,\vartheta_i,\varphi_s,\varphi_i)tg\vartheta_s d\vartheta_s d\varphi_s. \tag{30}$$

Taking this property into account, we now formulate the expression for the *intrinsically radiated* idler photons in the same way as Eq. (25) for the *intrinsically radiated* signal photons:

$$\langle N_i(L)\rangle=\left(\sum_s g_{si}\right)\langle N_q\rangle+(1-\kappa_i)\left(\sum_s g_{si}\right)\langle N_T\rangle+(1-e^{-2\mu_i L})\langle N_T\rangle. \tag{31}$$

The same parametric gain coefficient $g_{si}\equiv|U_{si}|^2=|U_{is}|^2$ enters both equations. Its distribution over idler (or signal) modes describes the divergence of parametrically generated idler (or signal, correspondingly) waves. The distribution accounts for both the inherent idler-wave absorption and the multimode character of the low-gain parametric process in a spatially limited crystal area.

The first terms in Eqs. (25) and (31) present results of the quantum SPDC effect. The SPDC contributions to populations of signal and idler modes are different. This occurs due to a loss coefficient and due to different spectrums of modes, over which the summation is done in Eqs. (25) and (31). The greater the difference between the frequencies of idler and signal photons, the greater the difference in angular divergence of active idler and signal modes. However, the total number of output SPDC signal photons, obtained after summation over

all output modes,

$$\sum_s \langle N_s(L)\rangle = \sum_{s,i} \kappa_s g_{si},$$

can be equal to a total number of output SPDC idler photons,

$$\sum_i \langle N_i(L)\rangle = \sum_{i,s} g_{si},$$

but only in the case of negligible absorption.

The second terms in Eqs. (25) and (31) describe the nonlinear parametric impacts of classical thermal field fluctuations (taken at the crystal temperature). These terms disappear if the crystal is transparent and $\kappa_s = \kappa_i = 1$. Obviously, such crystal cannot radiate from the classical point of view. Nevertheless, if absorption takes place (in our case at idler frequencies), the nonlinear-optical contributions from thermal fluctuations are nonzero both in the signal and idler parts. Starting from zero for zero absorption, both contributions grow when the absorption coefficient increases. The relative contribution of thermal fluctuations per unit $\langle N_T\rangle = 1$ changes with frequency as $(\kappa_s - 1)/\kappa_s$ in the case of intrinsic emission at signal frequency, and as $(1 - \kappa_i)$ in the case of intrinsic idler nonlinear emission. Figure 6 shows these dependencies calculated for 5-mm-long Mg:$LiNbO_3$. Finally, at high levels of absorption, quantum and thermal effective input photons ($\langle N_q\rangle \equiv 1$ and $\langle N_T\rangle$) are scaled with the same coefficients. In the case of the signal output photons $\langle N_s(L)\rangle$ this coefficient is $\kappa_s(\sum_i g_{si})$; in the case of the idler output photons $\langle N_i(L)\rangle$ it is $(\sum_s g_{si})$. However, at moderate values of the absorption parameter μ_i, the scaling coefficients for thermal fluctuations remain always less than the scaling coefficients for quantum fluctuations. This concerns both signal and idler output photons. However, taken at the same value of α_i, this difference is more pronounced for the signal photons. It is also noticeable that the greater the idler absorption coefficient and, correspondingly, the loss factor κ_s, the greater the difference between parametrically generated signal and idler photons.

Finally, the third term stands in Eq. (31) only since it is responsible for the classical linear Kirchhoff law. Indeed, the crystal is considered nonabsorptive at signal frequencies and, therefore, cannot emit signal radiation within the approximation of linear optics.

VII. CONCLUSIONS

We have studied peculiar properties of signal and idler photons generated under spontaneous PDC in the strongly frequency nondegenerate case, when the signal frequency is shifted from the frequency of the optical pump up to 0.1–2 THz. This mode is attractive because of the possibility of generating quantum-correlated optical-terahertz biphoton pairs. However, thermal idler field fluctuations, inherent absorption of THz radiation, and the multimode character of PDC in a spatially limited nonlinear volume can significantly change the properties of signal and idler photons generated in the strongly nondegenerate case. As a first step, in this paper we obtained expressions for specific frequency-angular distributions of photon numbers and power densities detected at signal and idler frequencies. Calculations were done in the low-gain limit without paraxial approximations, taking the Gaussian pump beam profile, and using the method of the generalized Kirchhoff law developed by Klyshko [20].

It is shown that transverse space constraints in the strongly frequency nondegenerate regime can cause a huge increase of the angular divergence of the output idler radiation. At the same time, inherent idler-wave absorption leads to an additional effect: the parametric conversion (gain) coefficients become different for internal field fluctuations and for the idler radiation incident from outside on a nonlinear crystal. Fortunately, the ratio between the conversion coefficients depends on absorption in approximately the same way for all the numerous spatial modes that are effectively involved in the parametric process. Therefore, with sufficient accuracy, influence of the two effects can be considered separately. Spatial limitation gives an angular shape of output idler radiation that is described by the angular response function S_ω presented by Eq. (16); the same function is responsible for angular resolution under detection of an external THz radiation by means of parametric frequency up-conversion. Absorption is manifested in the amplitudes of corresponding gain coefficients. The ratios between the coefficients in the signal and idler channels are defined by the THz-loss factors κ_s and κ_i, correspondingly. It is noteworthy that Eqs. (18) and (29), obtained independently for each factor, can be converted from one to another by simply changing the sign of the absorption coefficient, so that $\kappa_s(-\alpha_i) = \kappa_i(\alpha_i)$. The obtained general relations will help in choosing the optimal pump and crystal spatial parameters for detecting and generating more or less directed THz beams in thermal equilibrium conditions.

In addition, we studied specifically the structure of intrinsic emission of a crystal taken without any equilibrium or nonequilibrium contributions from external sources. GKL equations predict in this case the nonlinear emission in both signal and idler channels, and the background of idler photons emitted due to the linear Kirchhoff effect. The nonlinear emission in both channels consists of two types of contributions, one from the quantum field fluctuations and another one from the intrinsic thermal fluctuations at idler frequencies. We show that, in full agreement with fluctuation-dissipation logic, contributions from thermal fluctuations disappear if absorption is negligible. Equations (25) and (31) demonstrate how the relative impact of thermal fluctuations grows when absorption is increased. Finally, in the high absorption limit, the parametric gain coefficients become equal for quantum and thermal fluctuations. They also show that contribution of quantum noise to the total number of PDC-generated signal photons remains κ_s times more than the same contribution to the number of idler photons.

The results obtained here by the GKL method for PDC-generated photon numbers do not contradict the results of other treatments that have been done previously for simpler cases of nonabsorptive [19] or spatially unlimited [12] nonlinear volumes. They demonstrate reliability and convenience of this approach in solving more challenging tasks. In forthcoming work the same approach will be extended to analysis of the second-order correlation functions of the optical-terahertz biphotons.

ACKNOWLEDGMENT

This work was done under the financial support of the Russian Science Foundation (Grant No. 17-12-01134).

[1] D. Bouwmeester, A. Ekert, and A. Zeilinger, *The Physics of Quantum Information: Quantum Cryptography, Quantum Teleportation, and Quantum Computation* (Springer, New York, 2000).
[2] D. N. Klyshko, ZhETF Pis'ma **6**, 490 (1967) [JETP Lett. **6**, 23 (1967)].
[3] S. E. Harris, M. K. Oshman, and R. L. Byer, Phys. Rev. Lett. **18**, 732 (1967).
[4] D. Magde and H. Mahr, Phys. Rev. Lett. **18**, 905 (1967).
[5] A. S. Akhmanov, V. V. Fadeev, R. V. Khokhlov, and O. N. Chunaev, ZhETF Pis'ma **6**, 575 (1967) [JETP Lett. **6**, 85 (1967)].
[6] T. Brougham and S. M. Barnett, Phys. Rev. A **85**, 032322 (2012).
[7] M. V. Fedorov, Phys. Rev. A **93**, 033830 (2016).
[8] M. V. Chekhova, G. Leuchs, and M. Żukowski, Opt. Commun. **337**, 27 (2015).
[9] G. Kh. Kitaeva, Phys. Rev. A **76**, 043841 (2007).
[10] A. Pathak, J. Křepelka, and J. Peřina. Phys. Lett. A **377**, 2692 (2013).
[11] W.-M. Su, R. Chinnarasu, C.-H. Kuo, and C.-S. Chuu, Phys. Rev. A **94**, 033805 (2016).
[12] V. V. Kornienko, S. A. Germanskiy, G. K. Kitaeva and A. N. Penin, Int. J. Quantum Inform. **12**, 1560023 (2014).
[13] S. S. Dhillon, M. S. Vitiello, E. H. Linfield, A. G. Davies, M. C. Hoffmann, J. Booske, C. Paoloni, M. Gensch, P. Weightman, G. P. Williams *et al.*, J. Phys. D **50**, 043001 (2017).
[14] T. Nagatsuma, G. Ducournau, and C. C. Renaud, Nat. Photonics **10**, 371 (2016).
[15] C. Kübler, H. Ehrke, R. Huber, R. Lopez, A. Halabica, R. F. Haglund, Jr., and A. Leitenstorfer, Phys. Rev. Lett. **99**, 116401 (2007).
[16] G. Kh. Kitaeva, S. P. Kovalev, A. N. Penin, A. N. Tuchak, and P. V. Yakunin, J. Infrared Milli Terahz Waves **32**, 1144 (2011).
[17] G. Kh. Kitaeva, P. V. Yakunin, V. V. Kornienko, and A. N. Penin, Appl. Phys. B **116**, 929 (2014).
[18] C. H. Monken, P. H. Souto Ribeiro, and S. Pádua, Phys. Rev. A **57**, 3123 (1998).
[19] G. Kh. Kitaeva and V. V. Kornienko, Int. J. Quantum. Inform. **15**, 1740024 (2017).
[20] D. N. Klyshko, *Photons and Nonlinear Optics* (Gordon and Breach, New York, 1988).
[21] B. Huttner and S. M. Barnett, Phys. Rev. A **46**, 4306 (1992).
[22] S. Shwartz, R. N. Coffee, J. M. Feldkamp, Y. Feng, J. B. Hastings, G. Y. Yin, and S. E. Harris, Phys. Rev. Lett. **109**, 013602 (2012).
[23] K. Inoue, Opt. Commun. **383**, 69 (2017).
[24] A. Drezet, Phys. Rev. A **95**, 023831 (2017).
[25] M. L. Levin and S. M. Rytov, Zh. Eksp. Teor. Fiz. **65**, 1382 (1974) [JETP **38**, 688 (1974)].
[26] W. Wasilewski, A. I. Lvovsky, K. Banaszek, and C. Radzewicz, Phys. Rev. A **73**, 063819 (2006).
[27] D. B. Horoshko and M. I. Kolobov, Phys. Rev. A **88**, 033806 (2013).
[28] G. Kh. Kitaeva, D. N. Klyshko, and I. V. Taubin, Sov. J. Quantum Electron. **12**, 333 (1982).
[29] G. K. Kitaeva, I. I. Naumova, A. A. Mikhailovsky, P. S. Losevsky, and A. N. Penin, Appl. Phys. B **66**, 201 (1998).
[30] K. A. Kuznetsov, G. Kh. Kitaeva, S. P. Kovalev, S. A. Germansky, A. M. Buryakov, A. N. Tuchak, and A. N. Penin, Appl. Phys. B **122**, 223 (2016).
[31] W. Shi, Y. J. Ding, N Fernelius, and F. K. Hopkins, Appl. Phys. Lett. **88**, 101101 (2006).
[32] H. Minamide, S. Hayashi, K. Nawata, T. Taira, J. Shikata, and K. Kawase, J. Infrared Milli Terahz Waves **35**, 25 (2014).
[33] V. V. Kornienko, S. A. Savinov, Yu. A. Mityagin, and G. Kh. Kitaeva, Opt. Lett. **41**, 4075 (2016).
[34] V. V. Kornienko, G. Kh. Kitaeva, F. Sedlmeir, G. Leuchs, and H. G. L. Schwefel, APL Photonics **3**, 051704 (2018).